

The Strain-Hardening Behavior of TZAV-30 Alloy After Various Heat Treatments

S.X. Liang, L.X. Yin, L.Y. Zheng, M.Z. Ma, and R.P. Liu

(Submitted June 11, 2015; in revised form December 31, 2015; published online January 14, 2016)

The Ti-Zr-Al-V series titanium alloys with excellent mechanical properties and low density exhibit tremendous application potential as structural materials in aviation, automotive, and navigation industries. The strain-hardening behavior of Ti-30Zr-5Al-3V (wt.%, TZAV-30) alloy with various heat treatments is investigated in this study. Experimental results show that strain-hardening behavior of the examined alloy depends on the heat treatment process. The average strain-hardening exponent, n , is approximately 0.061 for WA specimen (825 °C/0.5 h/water quenching + 600 °C/4 h/air cooling), 0.068 for FC (850 °C/0.5 h/furnace cooling), 0.121 for AC (850 °C/0.5 h/air cooling), and 0.412 for WQ (850 °C/0.5 h/water quenching). Analysis of strain-hardening rate versus true strain curves indicates that higher n of AC specimen results from the lower degradation rate of strain-hardening rate with strain, and the ultrahigh n of WQ specimen is attributed to the evident increase in strain-hardening rate at the true strain from 0.04 to 0.06. Phase constitution and microstructural analyses reveal that the n of the examined alloy with $\alpha + \beta$ phases increases with the increase in the relative content of the retained β phase but is independent of average thickness of α plates. The increase in strain-hardening rate in WQ specimen depends on metastable α'' martensite and martensitic transition induced by tensile stress.

Keywords heat treatment, microstructure, strain hardening, titanium alloys

1. Introduction

Metal Ti and Ti alloys with low density, advantageous high special strength (σ/ρ , σ is the strength and ρ is the density), and favorable erosion resistance in numerous aggressive environments are widely applied in aviation, navigation, medical, chemical engineering, and other fields (Ref 1, 2). Given that the performance requirement in high-tech fields continues to increase, the development of new Ti alloys with high and ultrahigh properties is important (Ref 3, 4). Several TiZrAlV series alloys (abbreviated to TZAV alloys) with ultrahigh strength have been reported (Ref 5, 6). Two representative alloys, namely, TZAV-20 (Ref 7) and TZAV-30 (Ref 8), with ultrahigh special strength exceeding 340 MPa/(g/cm³) present tremendous application potential in aviation, automotive, navigation, and other fields.

However, the high cost of Ti alloys from difficulties in processing severely limits their practical applications (Ref 9). Thus, processability improvement has always been the focus for Ti alloys. Plastic forming processes are deeply dependent on strain-hardening behavior (Ref 10). Thus, research on strain-hardening behavior of Ti alloys is important for improving processability and promoting practical applications. Mechanical

properties largely depend on the phase constitution and microstructure. Wang (Ref 11) and Venkatesh (Ref 12) showed that the strain-hardening exponent (n) of Ti alloys decreases with the increase in strain rate and/or with the decrease in temperature. Zuo et al. (Ref 13) showed that the n of the ferrite-martensite dual-phase steels increases with the increasing martensite fraction. Ertorer et al. (Ref 14) showed that the n of pure Ti decreases with the decrease in average grain size. However, investigation on strain-hardening behavior of new TZAV series alloys is rare.

As mentioned, strain-hardening behavior of Ti alloys largely depends on phase constitution and microstructure, which can be controlled and adjusted effectively by plastic working and heat treatment. In the current paper, the phase constitution and microstructure of the TZAV-30 alloy were adjusted via heat treatment. Strain-hardening behavior of the TZAV-30 alloy with various phase constitution and microstructures was investigated. The influence mechanism of phase constitution and microstructure on strain-hardening behavior was also discussed. The current findings are beneficial to improve processability and promote the practical application of Ti alloys.

2. Experimental Procedure and Methods

Sponge Ti (99.7 wt.%), HZr-1 level sponge Zr (Zr + Hf \geq 99.5 wt.%, Hf \leq 3 wt.%), industrially pure Al (99.5 wt.%), and V (99.9 wt.%) were used to prepare alloy with the following composition in weight percentage: Ti-30Zr-5Al-3V (TZAV-30). The alloy was melted by ZHT-001 type vacuum-consumable electro-arc furnace, followed by cogging at 1050 °C and heat forging at 950 °C successively. The detailed preparation procedure is shown in Ref 15. Specimens with size of 10 mm \times 10 mm \times 70 mm (width \times height \times length) were sectioned as heat-treated specimens. Heat treatments were

S.X. Liang, L.X. Yin, and L.Y. Zheng, College of Equipment Manufacture, Hebei University of Engineering, Handan 056038, China; and M.Z. Ma and R.P. Liu, State Key Laboratory of Metastable Materials Science and Technology, Yanshan University, Qinhuangdao 066004, China. Contact e-mails: liangshx@hebeu.edu.cn and mz550509@ysu.edu.cn.

Table 1 Heat treatments performed on TZAV-30 alloy

Code	Heat treatments
FC	850 °C, 0.5 h, furnace cooling
AC	850 °C, 0.5 h, air cooling
WQ	850 °C, 0.5 h, water quench
WA	825 °C, 0.5 h, water quench + 600 °C, 4 h, air cooling

performed in a SK-G06143 tubular vacuum heat treatment furnace in a protective argon atmosphere. The detailed heat treatments are shown in Table 1. Bone-shaped plate specimens with a 21 mm gauge length, 3 mm gauge width, and 2 mm gauge thickness were prepared for tensile tests.

The phase constitution of the specimen with size of 10 mm × 10 mm × 5 mm was examined by x-ray diffraction (XRD) that uses Cu K α radiation [ASTM: D5380-93(2014)]. S-4800 type scanning electron microscopy (SEM) and JEM2010 type transmission electron microscopy (TEM) were used to test and/or analyze the microstructure. SEM specimens were prepared by using a typical quantitative metallographic method. The etching solution is a mixed solution (5 mL HF, 10 mL HNO₃, and 85 mL H₂O). TEM specimens were prepared by twin-jet electrochemical polishing in a solution of 10% perchloric acid and 90% methanol at 13 V and 238 K. Tensile tests were conducted on an Instron mechanical testing system at room temperature, and the strain rate was 5×10^{-4} /s in the range from 10^{-3} to 10^{-4} /s according to the ISO 6892-1:2009 (Ref 16). Strain throughout the entire testing process was monitored with an extensometer with 12.5 mm gauge length.

Statistical thickness distribution of α plate in various specimens is obtained from SEM or TEM micrographs by using standard test methods for determining average grain size (ASTM: E112-12). The volume fraction of the retained β phase was measured by point-counting method. The SEM/TEM micrograph was covered by a suitable grid. The percentage of the number of grid points located at the β phase in the total number of grid points was regarded as volume fraction of the retained β phase. The true stress-strain (S - e) curve was calculated from engineering stress-strain (σ - ϵ) curve using formulas $S = \sigma(1 + \epsilon)$ and $e = \ln(1 + \epsilon)$. Uniform plastic deformation is the deformation stage at true strain from e_e to e_b in S - e curve, where e_e and e_b are the true strain at elastic limit and ultimate tensile strength, respectively.

To avoid occasional results, all tests on each specimen were performed for a minimum of three times. The data points signed in the figures are the average values. The error bars in the figures show the relative deviations between the three repetitive results and average value.

3. Results

3.1 Microstructure of Specimens with Various Treatments

Figure 1 shows that the XRD patterns of TZAV-30 alloy underwent various heat treatments. Analysis reveals that FC, AC, and WA specimens are composed of a two-phase equilibrium of $\alpha + \beta$, whereas WQ specimen consists of major α'' martensite and several retained β phases. Previous reports (Ref 8, 17) also showed similar results, in which the phase

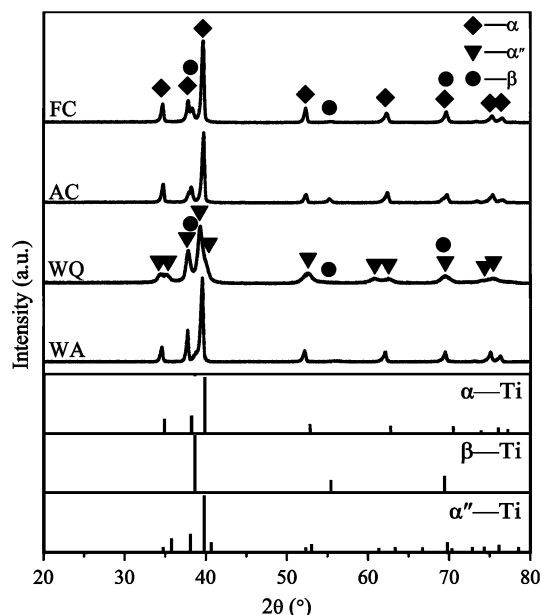


Fig. 1 The XRD patterns of the examined alloy with various heat treatments

constitution of annealed and aged TZAV-30 specimens is an equilibrium of two phases, $\alpha + \beta$.

Figure 2 shows the micrographs of TZAV-30 specimens with various heat treatments. The micrographs of Fig. 2(a) to (c) show that FC, AC, and WA specimens possess similar basket weave microstructures. However, the content of the retained β phase and grain size of α plate in the aforesaid three specimens are different. The microstructural feature of WQ specimen is characterized by major acicular α'' martensite and retained β phase, as shown in Fig. 2(d).

3.2 Strain-Hardening Behavior of Specimens with Various Treatments

Figure 3 shows the tensile results of TZAV-30 alloy with various heat treatments. True stress-strain (S - e) curves of various specimens are shown in Fig. 3(a). To investigate strain-hardening behavior, the uniform plastic deformation stage has been marked on each S - e curve. Holloman (Ref 18) showed that the relationship between S and e during uniform plastic deformation stage in the S - e curve of metal, and alloys can be expressed as $S = Ke^n$, where K is a constant and n is the strain-hardening exponent. According to the Holloman equation, the $\ln S - \ln e$ during uniform plastic deformation stage should be a straight line, and the n value is the slope of the straight line of $\ln S - \ln e$. The $\ln S - \ln e$ fitted straight line during the uniform plastic deformation stage of each examined specimen is obtained from the corresponding S - e curve, and all $\ln S - \ln e$ fitted straight lines are shown in Fig. 3(b). Thus, the n of various specimens can be obtained from Fig. 3(b). The average value is 0.068 for FC specimen, 0.121 for AC, 0.412 for WQ, and 0.061 for WA. The particular strain-hardening behavior of WQ specimen should result from the metastable α'' martensite. Previous results (Ref 19, 20) showed that the metastable α'' martensite in Ti alloys possesses low strength, low elastic modulus, and high strain-hardening exponent.

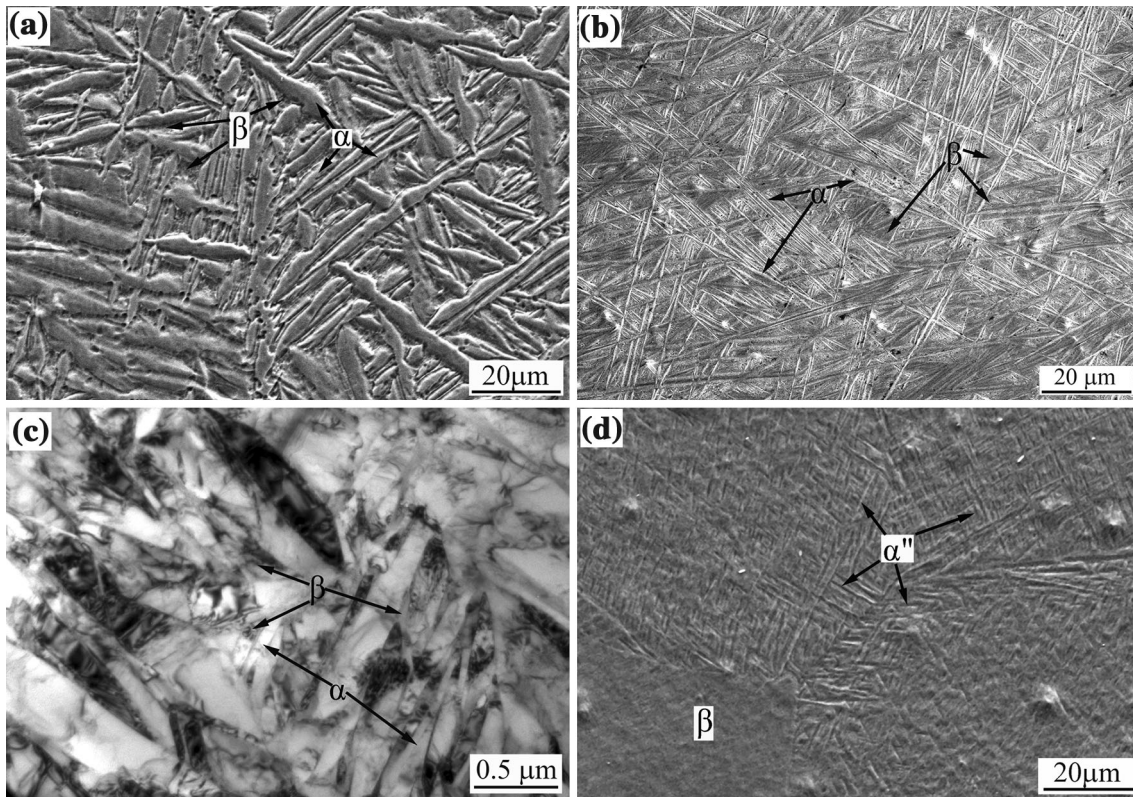


Fig. 2 Micrographs of specimens with various heat treatments (a) SEM of FC, (b) SEM of AC, (c) TEM of WA, and (d) SEM of WQ

4. Discussion

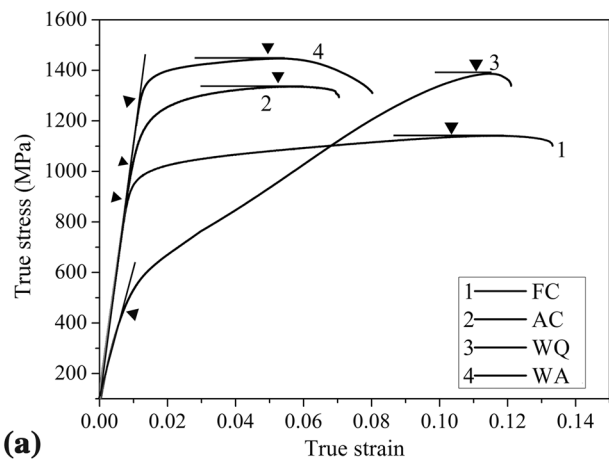
4.1 Effects of Phase Constitution on Strain-Hardening Exponent

As mentioned above, the strain-hardening exponent n of WQ specimen with α'' martensite and retained β phase is considerably higher than that of other specimens with two-phase $\alpha + \beta$ equilibrium. To investigate the effect of phase constitution on strain-hardening behavior, we obtained the strain-hardening rate versus true strain ($dS/de - e$) curve of each specimen from the corresponding $S - e$ curve; and all $dS/de - e$ curves are shown in Fig. 4(a). The FC, AC, and WA specimens with the same phase constitution present similar $dS/de - e$ curves, which can be characterized by three stages, as reported by Ahmad (Ref 21). The initial plastic deformation stage with high dS/de is defined as Stage I; the rapid decrease stage in $dS/de - e$ curve is Stage II; and in Stage III, the dS/de is almost a constant near zero. However, Salem et al. (Ref 22) showed a second hardening behavior after the rapid decrease (Stage II) in the $dS/de - e$ curve of pure α -Ti, as shown in Fig. 4(b); the second hardening behavior results from the formation of twins during plastic deformation. However, no twins can be found in the examined alloy during plastic deformation (Ref 23). Previous reports (Ref 24-26) also showed that the second hardening behavior in $dS/de - e$ curve of alloys with hexagonal close-packed (hcp) crystal structure is intimately linked with deformation twins. Won et al. (Ref 27) also proved that the strain hardening along rolling direction with twinning deformation is more evident than that along normal and transverse directions with dislocation slip in high purity Ti. The $dS/de - e$ curve of WQ specimen is also shown in Fig. 4(a).

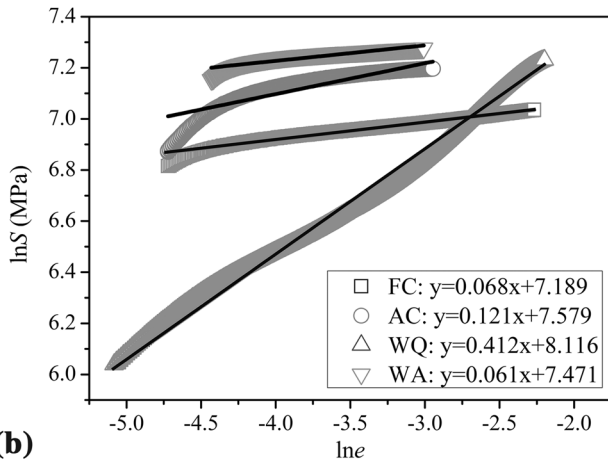
The $dS/de - e$ curve of WQ specimen is markedly different from that of FC, AC, and WA specimens but is similar with the curves in Fig. 4(b). However, the mechanism of second hardening behavior in the $dS/de - e$ curve of WQ specimen should not result in the formation of twins. Apart from the formation of twins, martensitic transition is another key factor of second hardening behavior in $dS/de - e$ curve. The previous result showed that martensitic transition induced by tensile stress in WQ specimen will occur (Ref 28). Neelakantan and Hanada et al. (Ref 29, 30) also revealed that martensitic transition induced by stress in Ti alloys with non-equilibrium phases can result in second hardening phenomenon (Ref 31, 32).

4.2 Effects of Phase Content on Strain-Hardening Exponent

According to XRD theory (Ref 33), the relative content of each phase in the multi-phase alloy presents a similar trend with the relative peak intensity of corresponding phase in the same XRD pattern. Thus, the trend of peak intensity ratio I_{β}/I_{α} in various treated specimens can indicate the trend of relative phase content. Here, I_{β} is a sign of (200) peak intensity of β phase near $2\theta = 55.2^{\circ}$, and I_{α} is a sign of (102) peak intensity of α phase near $2\theta = 52.3^{\circ}$. Based on the results of XRD, the I_{β}/I_{α} value is approximately 0.105 for FC specimen, 0.496 for AC and 0.086 for WA. Thus, the β phase content order from high to low is in the order of AC, WA, and FC specimens. Variations of n with I_{β}/I_{α} , as well as volume fraction of β phase (f_{β}), are shown in Fig. 5 and Table 2. The n value increases from 0.068 for FC specimen to 0.121 for AC with increasing I_{β}/I_{α} ratio from 0.105 to 0.496, and variation of n with f_{β} is similar to that with I_{β}/I_{α} ratio. A previous result (Ref 23) showed that



(a)



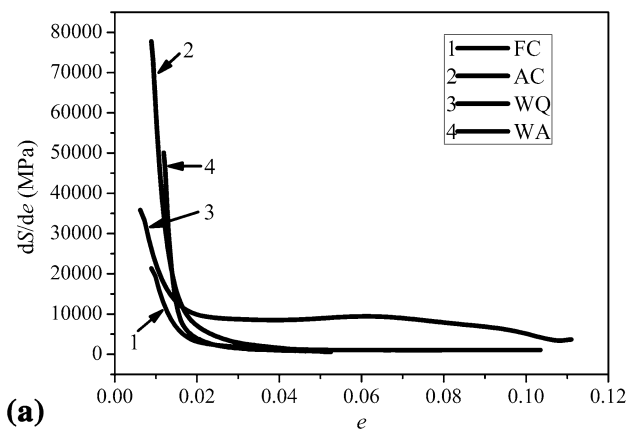
(b)

Fig. 3 Tensile results of TZAV-30 alloy with various heat treatments (a) S - e curves, the stage between two triangles marked on each curve is the uniform plastic deformation stage, (b) $\ln S$ - $\ln e$ curves of uniform plastic deformation stage and corresponding fitted straight lines

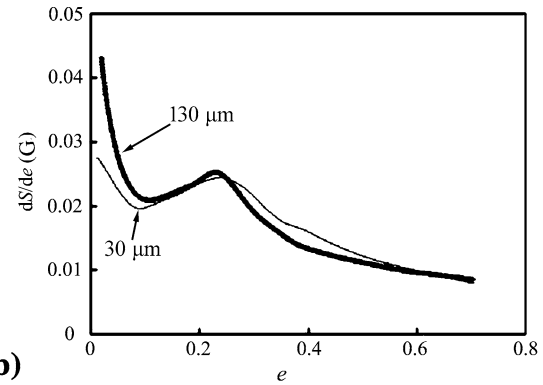
the plastic deformation mechanism of TZAV-30 alloy with $\alpha + \beta$ phases involves only dislocation glide. Thus, strain hardening of the examined alloy originates mainly from the accumulation of the forest of dislocations and their interaction (Ref 34, 35). In fact, the dislocation motion and multiplication during plastic deformation in β phase with bcc structure are easier and faster than that in the α phase with hcp structure. Therefore, the n value in the examined alloy with $\alpha + \beta$ phases is largely dependent on the content of the β phase. Kang et al. (Ref 36) also showed that deformation of β phase in Ti-4%Cr alloy caused significant strain hardening.

4.3 Effects of Grain Size on Strain-Hardening Exponent

Based on the micrographs in Fig. 2, variation of thickness (h) of α plate in WA, AC, and FC specimens with $\alpha + \beta$ phases and its effect on n are shown in Fig. 6. Statistical h distributions of α plate in Fig. 6(a) to (c) show that the h values are primarily around 0.35 μm for WA specimen, 0.85 μm for AC, and 4.2 μm for FC. Previous results (Ref 37, 38) showed that the strain-hardening behavior of metal and alloys depends on the microstructure parameters, such as grain size. Variation in n with average h of α plate in Fig. 6(d) and Table 2 reveals that the trend line of n versus h is a parabola, that is, n increases first



(a)



(b)

Fig. 4 The $dS/de - e$ curves of (a) the examined alloy with various treatments, (b) α -Ti with various grain sizes of 30 and 130 μm

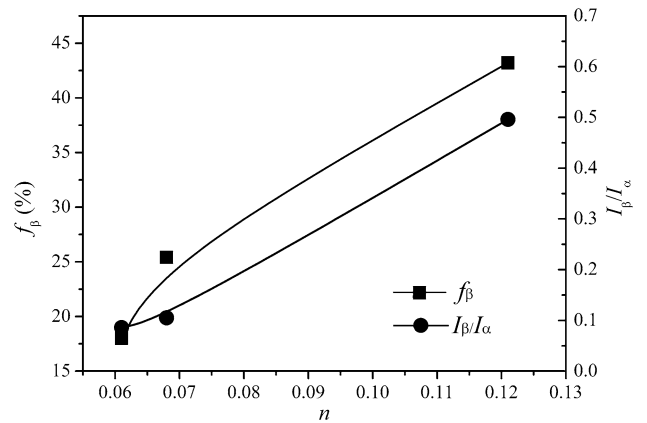


Fig. 5 Variations of n with relative phase content in specimens with $\alpha + \beta$ two phases

with the increase in h but then decreases with further increase in h . This trend is inconsistent with previous results (Ref 39, 40), which showed that n decreases gradually with increase in grain size. The key factor of this discrepancy is the relative content of β phase. According to section 4.2, strain-hardening behavior and the n value of the examined alloy depend greatly on the relative content of β phase. Thus, the influence of h on strain-hardening behavior is obscured by the relative content of β phase. Although the WA specimen possesses smaller h , the relative content of β phase in that specimen is also lower.

Table 2 Microstructure and strain-hardening exponent of specimens with various treatments

Specimen	PC	I_{β}/I_{α}	f_{β} (%)	h (μm)	n
FC	$\alpha + \beta$	0.105	29	4.2	0.068
AC	$\alpha + \beta$	0.496	43	0.85	0.121
WQ	$\alpha'' + \beta$	/	/	/	0.412
WA	$\alpha + \beta$	0.086	18	0.35	0.061

Note PC is the short form of phase constitution, and f_{β} is the volume fraction of retained β phase obtained from SEM/TEM micrographs

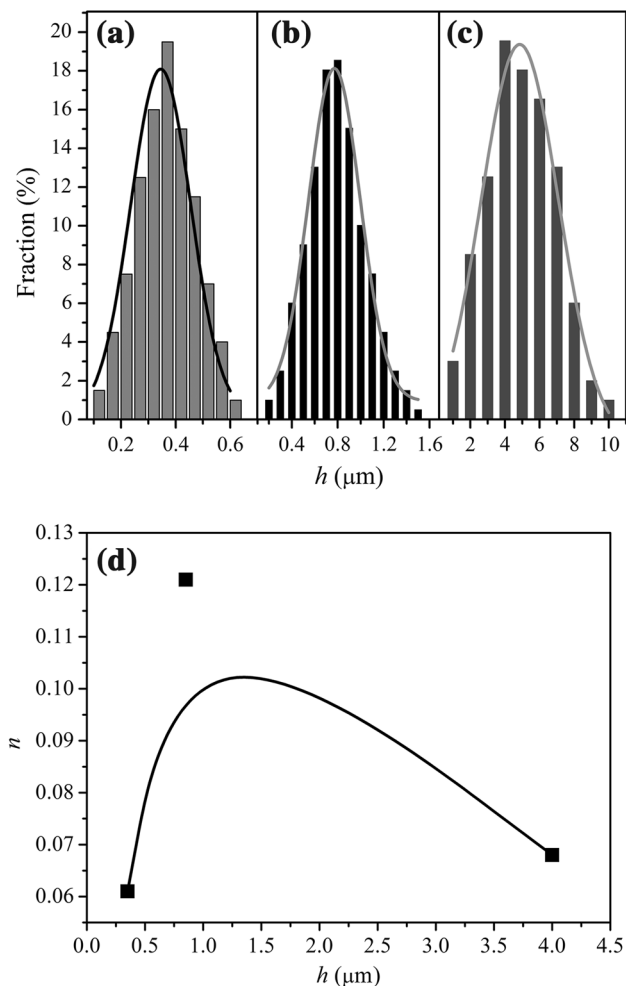


Fig. 6 Statistical h distributions of specimens (a) WA, (b) AC, (c) FC, and (d) the trend line of n vs. h of α plate

Therefore, n of WA specimen is lower than that of AC instead. Previous result (Ref 23) also revealed that the effect of grain size on the mechanical properties of the Ti alloy is obscured by the relative content of β phase and aspect ratio of the α plate.

5. Conclusions

The strain-hardening behavior of TZAV-30 alloy with various heat treatments is investigated in this work. The conclusions are summarized as follows:

- (1) The strain-hardening behavior of the examined alloy depends considerably on heat treatment. Strain-hardening exponent is approximately 0.061 for WA specimen, 0.068 for FC, 0.121 for AC, and 0.412 for WQ.
- (2) Metastable α'' martensite and phase transition induced by tensile stress can increase the strain-hardening exponent of TZAV-30 alloy significantly.
- (3) The relative content of β phase is a major factor of strain-hardening exponent of TZAV-30 alloy with $\alpha + \beta$ equilibrium phases instead of the thickness of the α plate.

Acknowledgment

This work was supported by the National Basic Research Program of China (Grant No. 2013CB733000), the National Natural Science Foundation of China (Grant Nos. 51271161/51401073/51434008/51421091), the Natural Science Foundation of Hebei Province of China (Grant No. E2014402014), and the Natural Science Foundation of Hebei Provincial Department of Education (Grant No. BJ2014017).

References

1. D. Banerjee and J.C. Williams, Perspectives on Titanium Science and Technology, *Acta Mater.*, 2013, **61**, p 844–879
2. Z. Huda and P. Edi, Materials Selection in Design of Structures and Engines of Supersonic Aircrafts: A Review, *Mater. Des.*, 2013, **46**, p 552–560
3. A. Ishida, M. Sato, and Z.Y. Gao, Effects of Ti Content on Microstructure and Shape Memory Behavior of $\text{Ti}_x\text{Ni}_{(84.5-x)}\text{Cu}_{15.5}$ ($x = 44.6\text{--}55.4$) Thin Films, *Acta Mater.*, 2014, **69**, p 292–300
4. Z.W. Chen, X.Z. Xiao, L.X. Chen, X.L. Fan, L.X. Liu, S.Q. Li, H.W. Ge, and Q.D. Wang, Development of Ti–Cr–Mn–Fe Based Alloys with High Hydrogen Desorption Pressures for Hybrid Hydrogen Storage Vessel Application, *Int. J. Hydrog. Energy*, 2013, **38**, p 12803–12810
5. S.X. Liang, M.Z. Ma, R. Jing, X.Y. Zhang, and R.P. Liu, Microstructure and Mechanical Properties of Hot-Rolled ZrTiAlV Alloys, *Mater. Sci. Eng. A*, 2012, **532**, p 1–5
6. R. Jing, S.X. Liang, C.Y. Liu, M.Z. Ma, X.Y. Zhang, and R.P. Liu, Structure and Mechanical Properties of Ti–6Al–4V Alloy After Zirconium Addition, *Mater. Sci. Eng. A*, 2012, **552**, p 295–300
7. R. Jing, S.X. Liang, C.Y. Liu, M.Z. Ma, and R.P. Liu, Aging Effects on the Microstructures and Mechanical Properties of the Ti–20Zr–6.5Al–4V Alloy, *Mater. Sci. Eng. A*, 2013, **559**, p 474–479
8. S.X. Liang, M.Z. Ma, R. Jing, Y.K. Zhou, Q. Jing, and R.P. Liu, Preparation of the ZrTiAlV Alloy with Ultra-High Strength and Good Ductility, *Mater. Sci. Eng. A*, 2012, **539**, p 42–47
9. MJ Donachie Jr., *Titanium: A Technical Guide*, ASM international, Metals Park, 1998
10. J.G. Eom, Y.H. Son, S.W. Jeong, S.T. Ahn, S.M. Jang, D.J. Yoon, and M.S. Joun, Effect of Strain Hardening Capability on Plastic Deforma-

- tion Behaviors of Material During Metal Forming, *Mater. Des.*, 2014, **54**, p 1010–1018
11. S.Q. Wang, J.H. Liu, and D.L. Chen, Effect of Strain Rate and Temperature on Strain Hardening Behavior of a Dissimilar Joint Between Ti–6Al–4V and Ti17 Alloys, *Mater. Des.*, 2014, **56**, p 174–184
 12. B.D. Venkatesh, D.L. Chen, and S.D. Bhole, Effect of Heat Treatment on Mechanical Properties of Ti–6Al–4V ELI Alloy, *Mater. Sci. Eng. A*, 2009, **506**, p 117–124
 13. X.R. Zuo, Y.B. Chen, and M.H. Wang, Study on Microstructures and Work Hardening Behavior of Ferrite-Martensite Dual-Phase Steels with High-Content Martensite, *Mater. Res.*, 2012, **15**, p 915–921
 14. O. Ertorer, T. Topping, Y. Li, W. Moss, and E.J. Laverni, Enhanced Tensile Strength and High Ductility in Cryomilled Commercially Pure Titanium, *Scr. Mater.*, 2009, **60**, p 586–589
 15. S.X. Liang, M.Z. Ma, R. Jing, C.L. Tan, and R.P. Liu, Structural Evolution and Mechanical Properties of Zr–45Ti–5Al–3V Alloy by Heat Treatments, *Mater. Sci. Eng. A*, 2012, **541**, p 67–72
 16. ISO, 6892-1, *Metallic Materials: Tensile Testing—Part 1: Method of Test at Room Temperature*, ISO, Brussels, 2009
 17. S.X. Liang, L.X. Yin, R. Jing, X.Y. Zhang, M.Z. Ma, and R.P. Liu, Structure and Mechanical Properties of the Annealed TZAV-30 Alloy, *Mater. Des.*, 2014, **58**, p 368–373
 18. J.H. Hollomon, Tensile Deformation, *Trans. AIME*, 1945, **162**, p 268–290
 19. M. Premkumar and A.K. Singh, Deformation Behavior of an Ordered B2 Phase in Ti–25Al–25Zr Alloy, *Intermetallics*, 2010, **18**, p 199–201
 20. Z. Yu and L. Zhou, Influence of Martensitic Transformation on Mechanical Compatibility of Biomedical β Type Titanium Alloy TLM, *Mater. Sci. Eng. A*, 2006, **391**, p 438–440
 21. E. Ahmad, T. Manzoor, and N. Hussain, Thermomechanical Processing in the Intercritical Region and Tensile Properties of Dual-Phase Steel, *Mater. Sci. Eng. A*, 2009, **508**, p 259–265
 22. A.A. Salem, S.R. Kalidindi, R.D. Doherty, and S.L. Semiatin, Strain Hardening Due to Deformation Twinning in α -Titanium: Mechanisms, *Metall. Mater. Trans. A*, 2006, **37**, p 259–268
 23. S.X. Liang, L.X. Yin, R. Jing, X.Y. Zhang, M.Z. Ma, and R.P. Liu, Deformation Mechanisms of a ZrTiAlV Alloy with Two Ductile Phases, *J. Mater. Res.*, 2013, **28**, p 2715–2719
 24. N. Tahreen, D.F. Zhang, F.S. Pan, X.Q. Jiang, C. Li, D.Y. Li, and D.L. Chen, Influence of Yttrium Content on Phase Formation and Strain Hardening Behavior of Mg–Zn–Mn Magnesium Alloy, *J. Alloys Compd.*, 2014, **615**, p 424–432
 25. B.S. Wang, R.L. Xin, G.J. Huang, and Q. Liu, Effect of Crystal Orientation on the Mechanical Properties and Strain Hardening Behavior of Magnesium Alloy AZ31 During Uniaxial Compression, *Mater. Sci. Eng. A*, 2012, **534**, p 588–593
 26. D. Sarker and D.L. Chen, Detwinning and Strain Hardening of an Extruded Magnesium Alloy During Compression, *Scr. Mater.*, 2012, **67**, p 165–168
 27. J.W. Won, C.H. Park, S.G. Hong, and C.S. Lee, Deformation Anisotropy and Associated Mechanisms in Rolling Textured High Purity Titanium, *J. Alloys Compd.*, 2015, **651**, p 245–254
 28. S.X. Liang, L.X. Yin, X.Y. Liu, X.L. Zhang, M.Z. Ma, R.P. Liu, and C.L. Tan, Microstructure Evolution and Mechanical Properties Response of a TZAV Alloy During Combined Thermomechanical Treatments, *Mater. Sci. Eng. A*, 2014, **619**, p 87–94
 29. S. Neelakantan, E.I. Galindo-Nava, D.S. Martin, J. Chao, and P.E.J. Rivera-Díaz-del-Castillo, Modelling and Design of Stress-Induced Martensite Formation in Metastable β Ti Alloys, *Mater. Sci. Eng. A*, 2014, **590**, p 140–146
 30. S. Hanada, N. Masahashi, and T.K. Jung, Effect of Stress-Induced α' Martensite on Young's Modulus of β Ti-33.6Nb-4Sn Alloy, *Mater. Sci. Eng. A*, 2013, **588**, p 403–410
 31. Z. Wyatt and S. Ankem, The Effect of Metastability on Room Temperature Deformation Behavior of β and $\alpha + \beta$ Titanium Alloys, *J. Mater. Sci.*, 2010, **45**, p 5022–5031
 32. C. Li, J.H. Chen, X. Wu, W. Wang, and S. Zwaag, Tuning the Stress Induced Martensitic Formation in Titanium Alloys by Alloy Design, *J. Mater. Sci.*, 2012, **47**, p 4093–4100
 33. R.J. Hill and C.J. Howard, Quantitative Phase Analysis from Neutron Powder Diffraction Data Using the Rietveld Method, *J. Appl. Cryst.*, 1987, **20**, p 467–474
 34. U.F. Kocks and H. Mecking, Physics and Phenomenology of Strain Hardening: The FCC Case, *Prog. Mater. Sci.*, 2003, **48**, p 171–273
 35. J.H. Lee, T.B. Holland, A.K. Mukherjee, X.H. Zhang, and H.Y. Wang, Direct Observation of Lomer-Cottrell Locks During Strain Hardening in Nanocrystalline Nickel by In Situ TEM, *Sci. Rep.*, 1061, **2013**(3), p 1–6
 36. D.S. Kang, N. Koga, M. Sakata, N. Nakada, T. Tsuchiyama, and S. Takaki, Enhanced Work Hardening by Redistribution of Oxygen in ($\alpha + \beta$)-Type Ti–4Cr–0.2O Alloys, *Mater. Sci. Eng. A*, 2014, **606**, p 101–107
 37. D.K. Yang, P.D. Hodgson, and C.E. Wen, Simultaneously Enhanced Strength and Ductility of Titanium Via Multimodal Grain Structure, *Scr. Mater.*, 2010, **63**, p 941–944
 38. Y.H. Zhao, X.Z. Liao, S. Cheng, E. Ma, and Y.T. Zhu, Simultaneously Increasing the Ductility and Strength of Nanostructured Alloys, *Adv. Mater.*, 2006, **18**, p 2280–2283
 39. R.Z. Valiev, R.K. Islamgaliev, and I.V. Alexandrov, Bulk Nanostructured Materials from Severe Plastic Deformation, *Prog. Mater. Sci.*, 2000, **45**, p 103–189
 40. Q. Wei, L. Kecskes, T. Jiao, K.T. Hartwig, K.T. Ramesh, and E. Ma, Adiabatic Shear Banding in Ultrafine-Grained Fe Processed by Severe Plastic Deformation, *Acta Mater.*, 2004, **52**, p 1859–1869